Solar Flare Effects on 150-km Echoes Observed Over Jicamarca: WACCM-X Simulations

N. M. Pedatella[1,2], J. L. Chau[3], J. Vierinen[4], L. Qian[1], P. Reyes[5], E. Kudeki[6], G. Lehmacher[7], and M. Oppenheim[8]

[1]High Altitude Observatory, National Center for Atmospheric Research, Boulder, CO, USA.
[2]COSMIC Program Office, University Center for Atmospheric Research, Boulder, CO, USA.
[3]Leibniz Institute of Atmospheric Physics, Rostock University, Kühlungsborn, Germany.
[4]Department of Physics and Technology, University of Tromsø, Tromsø, Norway
[5]Center for Geospace Studies, SRI International, Menlo Park, California, USA
[6]Department of Electrical and Computer Engineering, University of Illinois at Urbana-Champaign,
[7]Department of Physics and Astronomy, University of Clemson, Clemson, SC, USA.
[8]Center for Space Physics, Boston University, Boston, MA, USA.

Key Points:

- There is a good agreement between observed morphology of 150-km echoes and simulated electron densities during a solar flare.
- The results support the hypothesis that layering of 150-km echoes is connected to electron densities.
- Decrease in vertical plasma drift during the solar flare can be attributed to changes in E-region conductivity.

Corresponding author: Nicholas Pedatella, nickp@ucar.edu

Abstract

Jicamarca Radio Observatory observations and Whole Atmosphere Community Climate Model with thermosphere-ionosphere eXtension (WACCM-X) simulations are used to investigate the effects of the September 7, 2005 X-17 solar flare on 150-km echoes, electron densities, and vertical plasma drifts. The solar flare produces a remarkably similar response in the observed 150-km echoes and simulated electron densities. The results provide additional evidence of the relationship between the background electron density and the layering structure that is seen in 150-km echoes. The simulations also capture a similar rapid decrease in vertical plasma drift velocity that is seen in the observations. The simulated change in vertical plasma drift is, however, weaker than the observed decrease at the longitude of Jicamarca, though it is stronger east of Jicamarca. The effect of the solar flare on the vertical plasma drifts is **primarily** attributed to changes in conductivity due to the enhanced ionization during the solar flare.

1 Introduction

Despite being first observed over 50-years ago (Balsley, 1964), the source of the enhanced VHF radar echoes that are observed near 150 km remains unexplained. These so-called 150-km echoes have subsequently been observed in the equatorial ionosphere at multiple longitudinal locations (J. L. Chau & Kudeki, 2006; Kudeki et al., 1998; de Paula & Hysell, 2004; Tsunoda & Ecklund, 2008; Choudhary et al., 2004; A. K. Patra et al., 2008). The 150-km echoes are observed nearly every day, and they are thus a ubiquitous feature of the equatorial ionosphere. The characteristics of the 150-km echoes have been well documented by observations. These characteristics include their occurrence only during the daytime, a necklace-like shape with descending structures prior to noon and ascending structures after noon, as well as the formation of distinct layers. Moreover, the majority of 150-km echoes are a manifestation of naturally enhanced incoherent scatter echoes (e.g., J. L. Chau, 2004; J. Chau et al., 2009; J. L. Chau & Kudeki, 2013). Some of these features have led to the hypothesis that the 150-km echoes are due to photoelectrons (e.g., Oppenheim & Dimant, 2016). The connection to photoelectrons is further supported by the absence of 150-km echoes during the January 2010 solar eclipse (A. K. Patra et al., 2011), as well as their modification by solar flares (Reyes, 2012).

The photoelectron origin of the 150-km echoes cannot fully explain the formation of several distinct layers. There does, however, appear to be a connection between the electron density, the temporal and altitudinal structure of the layers, and the gaps that form between layers (e.g., J. L. Chau et al., 2009; Reyes, 2017). For example, Reyes (2017) show a close correspondence between short-period (∼5-10 minute) fluctuations in electron densities and the gaps in the 150-km echoes. This has led to the suggestion that the gaps between layers may form at distinct plasma frequencies (e.g., G. Lehmacher et al., 2018). However, A. Patra et al. (2017) recently disputed the connection between photoelectrons and 150-km echoes. They found an inverse relationship between 150-km echo power and EUV flux, and hypothesized that neutral dynamics play an important role in the formation of 150-km echoes. Though neutral dynamics may contribute to the 150-km echoes, they would not fully explain features such as the daytime only occurrence, narrow spectral widths, solar eclipse, and solar flare effects. These features suggest that photoelectrons contribute to the formation of 150-km echoes.

Nonetheless, the connection between 150-km echoes, photoelectrons, and electron densities has yet to be fully explored. Understanding the relationship between 150-km echoes and electron densities would provide an additional step towards developing a complete theory to explain the 150-km echoes, improving our understanding of the equatorial ionosphere. If a relationship between electron density and the power striations can be determined, 150-km echoes could also provide a high signal-to-noise ratio radar tar-

get for accurately measuring the electron density between the E-region and the F-region of the ionosphere.

The main objective of the present study is to further investigate the connection between electron densities and the 150-km echo layers. This is done through a comparison of Jicamarca Radio Observatory (JRO) observations of 150-km echoes during the September 7, 2005 solar flare with electron densities simulated in the Whole Atmosphere Community Climate Model with thermosphere-ionosphere eXtension (WACCM-X). The simulated electron densities closely follow the observed layering structure of the 150-km echoes, supporting the close connection between the electron densities and the gaps that form between the 150-km echo layers. We further investigate the change in vertical plasma drift velocity during the solar flare, and find that this is likely related to a rapid change in the conductivity that occurs during the solar flare.

2 JRO Observations

The JRO observations were taken as part of a MST-ISR experiment, which is an experiment designed to observe the Mesosphere, Stratosphere and Troposphere (MST) at the same time as the ionosphere in quasi thermal equilibrium via the Incoherent Scatter Radar (ISR) mode (e.g., G. A. Lehmacher et al., 2009, 2019). The MST mode allows the observation from 0 km to 200 km, while the ISR mode measures from 200 km to 900 km in altitude. Although the mesosphere stops at around 100 km, the MST mode has proven to also be useful in the study of coherent scattering from ionospheric irregularities, such as those coming from 150-km echoes (e.g., Kudeki & Fawcett, 1993; J. L. Chau & Kudeki, 2006). The MST-ISR mode is realized by interleaving sequences of pulses with different repetition, pulse width and pulse coding. In the case of the MST part, 20 consecutive pulses with 1.33 ms (or ∼200 km) interpulse period (IPP) and 64 baud complementary codes pulses with a total width of 64 μs (or 9.6 km) are transmitted. In the case of the ISR part, 2 Barker-3 coded pulses with a total width of 300 μs (or 45 km) and an IPP of 6.66 ms (or ∼1000 km) were transmitted. **The nominal range resolution of the observations is 150 m.**

These pulse sequences were transmitted simultaneously on four different beam positions (North, East, South and West), taking advantage of the modular and polarization features of JRO. Two transmitters of 1 MW peak power each, were combined before feeding all four beams simultaneously, i.e., on each beam 500 kW peak power was transmitted. In this work we present the results of September 7, 2005 only from the MST part of the West beam (-87.68° azimuth, 87.52° elevation), which is the beam pointing the closest to perpendicular to the Earth's magnetic field **B** (beam gain peak ∼0.8° from perpendicular to **B** and elongated in the North-South direction with a beam width of ∼1.4°) at 150 km at the time of the experiment. More details of the JRO modes, signal processing, other solar flare effects, and other events can be found in Reyes (2012).

3 WACCM-X

Model simulations are performed in WACCM-X version 2.0 (H.-L. Liu et al., 2018). WACCM-X extends from the surface to the upper thermosphere (4.1×10^{-10} hPa, ∼500-700 km depending on solar activity), and has a resolution of 1.9° in latitude, 2.5° in longitude, and 0.25 scale heights above the stratosphere. Up to the lower thermosphere, WACCM-X is based on the Community Atmosphere Model (CAM) version 4 (Neale et al., 2013) and Whole Atmosphere Community Climate Model (WACCM) version 4 (Marsh et al., 2013). Upper atmospheric processes, including the transport of O^+, self-consistent ionospheric electrodynamics, and energetics included in WACCM-X are primarily based on the Thermosphere-Ionosphere-Electrodynamics General Circulation Model (TIE-GCM) (Roble et al., 1988; Richmond et al., 1992). H.-L. Liu et al. (2018) and J. Liu et al. (2018) provide a detailed description and validation, respectively, of WACCM-X version 2.0

For the model simulations in the present study, the specified dynamics approach (Smith et al., 2017) is used to constrain the lower atmosphere meteorology up to 50 km to the National Aeronautics and Space Administration (NASA) Modern Era Retrospective Analysis for Research and Applications version 2 (MERRA-2) (Gelaro et al., 2017). Geomagnetic forcing is incorporated by imposing the Heelis empirical convection pattern at high latitudes (Heelis et al., 1982), which is driven by the 3-hr geomagnetic K_p index. The Flare Irradiance Spectral Model (FISM) (Chamberlin et al., 2008) provides the solar spectral irradiance for the solar flare that occurred on September 7, 2005. FISM is an empirical model that uses observational data from Geostationary Operational Environmental Satellite (GOES) X-Ray Sensor (XRS), Thermosphere Ionosphere Mesosphere Energetics and Dynamics (TIMED) Solar Extreme Ultraviolet Experiment (SEE), and Solar Radiation and Climate Experiment (SORCE) SOlar Stellar Irradiance Comparison Experiment (SOLSTICE) to estimate the solar irradiance at wavelengths from 0.1 to 190 nm at 60 s temporal resolution. FISM is thus able to capture the solar irradiance variability during solar flares at wavelengths that directly impact the ionosphere and thermosphere, which includes the soft X-rays (0.1-10 nm) and extreme ultraviolet (EUV, 10-121.6 nm). Previous studies have demonstrated that the solar flare irradiance information provided by FISM is suitable for studying the effects of solar flares in the mesosphere, thermosphere, and ionosphere (e.g., Qian et al., 2011; Pettit et al., 2018).

4 Results and Discussion

4.1 Flare Impact on 150-km Echoes and Electron Density

The signal to noise ratio (SNR) observed by JRO on September 7, 2005 is shown in Figure 1a. The X-ray flux observed by GOES XRS is shown in Figure 1c. An X-17 solar flare began at 17:17 UT, reached its maximum intensity at 17:40 UT, and the solar irradiance returned to nominal levels over the next ∼1 hour. Prior to the solar flare, the characteristic behavior of 150-km echoes is observed, with gradually descending layers of enhanced SNR that are 5-10 km thick. The enhanced SNR layers are separated by gaps that are on the order of a kilometer thick. The layers descend rapidly in altitude beginning around 17:30 UT, which corresponds to the **time when the X-ray enhancement was observed by the GOES satellite**. After the flare, around 18:00 UT, the layers initially rise rapidly, though the rate of ascent slows over the following hour. The vertical thickness of the layers also appears to be changed by the solar flare, with the layers being narrower following the solar flare.

The corresponding electron densities simulated by WACCM-X are shown in Figure 1b. Note that the WACCM-X results have been shifted later by 5 minutes to be more consistent with the observations. This corresponds to the model time step, as well as the solar flare forcing input, so we consider a 5 minute offset to not be a significant discrepancy between the timing of the solar flare effects in the observations and simulations. We also note that the coarse (relative to solar flare time scales) time step of WACCM-X may tend to smooth the model response to the solar flare. Contours of constant electron density in the WACCM-X simulations exhibit many of the same features that are seen in the observations. Prior to the flare, the electron density contours can be seen to largely track the gaps and edges in the radar echoes. The exception being the smaller scale structures that are seen in the observations, which are attributed to gravity waves that are unresolved in WACCM-X. The consistency between the Jicamarca observations and WACCM-X simulations is especially apparent during the solar flare. In particular, both show a rapid descent in altitude beginning around 17:30 UT, followed by a more gradual ascent around 18:00 UT. The electron density contours are additionally more closely spaced following the flare, a feature consistent with the JRO SNR observations.

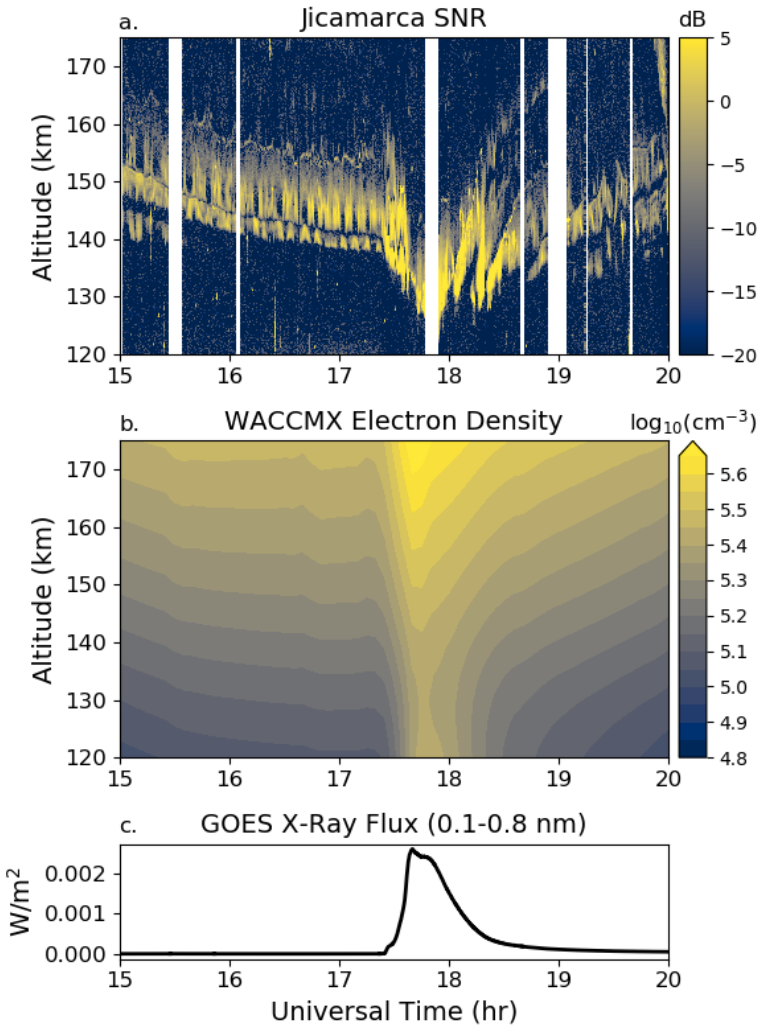

Figure 1. (a) JRO observed signal to noise ratio (SNR) during the September 7, 2005 solar flare. White areas indicate time periods without observations. (b) Electron densities simulated by WACCM-X at the location of Jicamarca, Peru. (c) Observed GOES x-ray flux for 0.1-0.8 nm.

To better illustrate the relationship between the 150-km echoes observed by JRO and the electron density simulated by WACCM-X, the two are plotted together in Figure 2 for a shorter time interval around the solar flare. The remarkable agreement in the effect of the solar flare on contours of constant electron density and the structure of the 150-km echo layers can be clearly seen in Figure 2. From Figure 2, it is apparent that the gaps in the 150-km echoes seem to follow electron density contours; however, the reason for this relationship is not yet known. With plasma-lines, there is a matching condition between plasma-frequency, radar wavelength, and suprathermal electron velocity (photoelectrons and auroral secondary electrons), which results in electron density dependent plasma-line radar echo enhancements (Perkins et al., 1965). The fact that this also occurs for the 150-km echoes, points to a similar wave-particle interaction (Oppenheim & Dimant, 2016). An alternative possibility is that the observed layering is related to gyro-harmonics (G. Lehmacher et al., 2018), though this would not explain the formation of multiple layers in the E-region because there are only two contours in the E-region where the electron density plasma frequency is an integer multiple of the gyro-frequency.

Thus, although the results demonstrate a close connection between electron density and the 150-km echo layers, the reason for this relationship remains unknown. Both of the previously mentioned hypotheses will be explored in detail in a future work, where comparisons between JRO observations and WACCM-X simulations under nominal (i.e., non-flare) conditions will be considered.

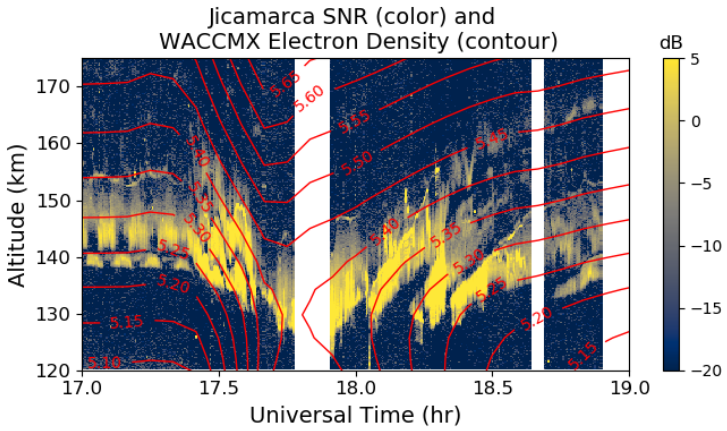

Figure 2. Observed signal to noise ratio (SNR) (colors), and WACCM-X electron densities in units of $\log_{10}\mathrm{cm}^{-3}$ (contours) during the September 7, 2005 solar flare.

4.2 Flare Impact on Vertical Plasma Drifts

In addition to influencing the E-region electron densities and 150-km echoes, solar flares can modulate the electrodynamics of the ionosphere (Qian et al., 2012; Zhang et al., 2017). As seen in Figure 3, the JRO observations of vertical plasma drift velocity (blue) show a clear response to the solar flare, and the drifts exhibit a sudden $\sim$15 ms^{-1} decrease at the onset of the solar flare. The WACCM-X simulations only exhibit a weak (1-2 ms^{-1}) response to the solar flare at 285°E geographic longitude (black). However, a stronger response occurs in the WACCM-X simulations at 320°E geographic longitude (red), though it is still slightly weaker than seen in the observations. Nonetheless, the vertical plasma drift response at 320°E is generally consistent with the JRO observations, and we can thus use the simulations to understand the mechanism behind the rapid decrease in the vertical plasma drift during the solar flare.

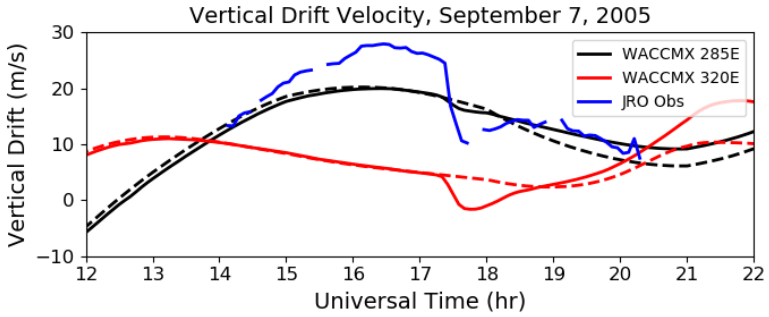

Figure 3. Equatorial vertical drift velocity on September 7, 2005 from Jicamarca 150-km echoes (blue), and WACCM-X simulations at 285°E (black) and 320°E (red) geographic longitude. Dashed lines indicate WACCM-X results without inclusion of the solar flare.

Previous studies investigating the solar flare effects on electrodynamics, and ionospheric currents, have attributed the response to a change in the ionospheric conductivity (Qian et al., 2012; Annadurai et al., 2018) and/or penetration electric field due to the imbalance of high latitude region-1 and region-2 field aligned currents. The later mechanism was proposed by Zhang et al. (2017) as a source of the decrease in vertical plasma drift observed during the September 7, 2005 solar flare. The WACCM-X simulation does not include the effects of penetration electric fields, and we therefore attribute the change in vertical plasma drifts to changes in the ionospheric conductivity. It should be noted that we cannot entirely discount effects of penetration electric fields, and inclusion of penetration electric fields could lead to a larger vertical plasma drift response. The fact that the WACCM-X simulations capture a decrease in vertical plasma drifts at 320°E does, however, indicate that conductivity changes are an important mechanism by which solar flares influence electrodynamics.

The changes in the WACCM-X Hall (σ_H) and Pedersen (σ_P) conductivities at 17:45 UT are shown in Figure 4 for 285°E and 320°E geographic longitude. Note that the changes are calculated relative to a WACCM-X simulation that did not include the solar flare forcing. For reference, maximum Hall and Pedersen conductivities at this time in the WACCM-X simulation without the solar flare are $\sim 8\times10^{-4}$S/m and $\sim 5\times10^{-4}$S/m, respectively. The conductivity changes due to the solar flare are thus large compared to the background conductivities. The corresponding zonal winds are shown in Figures 4c and 4f. Note that the zonal winds are largely unchanged by the solar flare below ~175 km, and are enhanced by 5-10 ms^{-1} above 200 km (not shown). The change in Hall conductivity due to the flare is larger at 285°E than it is at 320°E, which should contribute to a larger decrease in the daytime eastward electric field, and thus a larger decrease in the vertical drift at 285°E. The change in Pedersen conductivity due to the solar flare is generally similar at the two longitudes. The background zonal winds are, however, notably different which is likely due to the differences in local time at the two longitudes (12:45 SLT at 285°E and 15:05 SLT at 320°E). We therefore attribute the smaller change in the simulated drift response at 285°E to be due to the zonal winds at the time of the solar flare, and it is possible that WACCM-X does not capture the flare effects at 285°E due to deficiencies in the zonal winds. These differences highlight the need to accurately simulate both the neutral winds and conductivities in order to accurately simulate the solar flare effects on ionospheric electrodynamics.

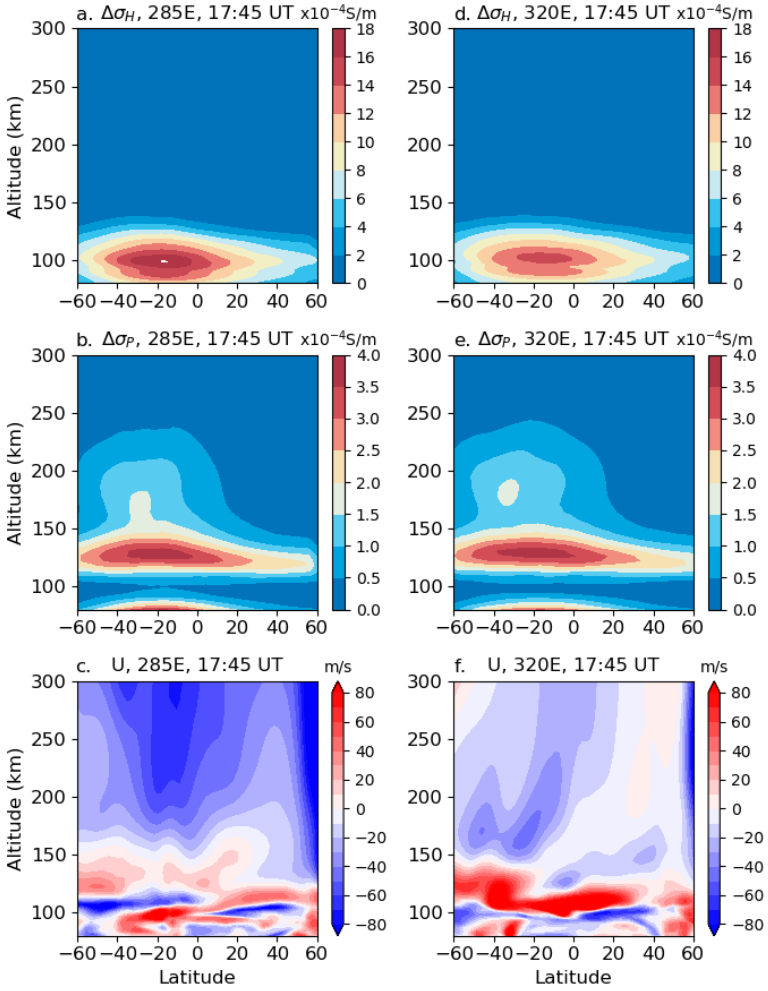

Figure 4. Changes in (a) Hall and (b) Pedersen conductivity at 285°E geographic longitude and 17:45 UT. (c) Zonal wind at 285° geographic longitude and 17:45 UT. (d-f) Same as (a-c) except for at 320°E geographic longitude.

5 Conclusions

The present study investigates the effects of the September 7, 2005 X-17 solar flare on the equatorial ionosphere using a combination of JRO observations and WACCM-X simulations. The solar flare is found to produce similar changes in the layering structure of observed 150-km echoes and simulated electron densities. In particular, both reveal a rapid descent at the onset of the solar flare, followed by a gradual ascent following the solar flare. The 150-km echo layers and contours of constant electron density are also both found to be narrower in vertical extent following the solar flare. These similarities support a connection between the background electron density and the layering structure that is seen in 150-km echoes. The reason for this relationship does, however, remain unknown, and further investigations into this connection will help in understanding the mechanisms that form the still unexplained 150-km echoes. The results also demonstrate that relatively coarse resolution whole atmosphere-ionosphere general circulation models, such as WACCM-X, can provide insight into smaller-scale structures in the equatorial ionosphere. This represents a new application of such models, enabling

potential future investigations focused on understanding, for example, the day-to-day variability of 150-km echoes.

The effect of the solar flare on the equatorial vertical plasma drifts was also investigated. The JRO observations show a sudden decrease in vertical plasma drift velocity of 15-20 ms^{-1} after the onset of the solar flare. The WACCM-X simulations reproduce a decrease in vertical plasma drift at 320°E geographic longitude, but only a weak (1-2 ms^{-1}) decrease at the longitude of Jicamarca (285°E). The vertical plasma drift changes are **primarily** attributed to changes in the conductivity in the simulations, which changes the daytime eastward electric field, and the longitudinal differences may be related to differences in the zonal winds at the time of the solar flare. This demonstrates that simulating the electrodynamic effects of solar flares requires accurately simulating both the zonal winds as well as the conductivities. **Penetration electric fields may also influence the response of the equatorial vertical plasma drifts to the solar flare, though the present results suggest that this may be a secondary effect.**

Acknowledgments

WACCM-X is part of the Community Earth System Model (CESM) and the source code is available at http://www.cesm.ucar.edu. The WACCM-X simulation output, and Jicamarca SNR observations, used in this publication are available at https://doi.org/10.26024/ahcm-6d40. The GOES x-ray observations are available from NASA NCEI **(https://www.ngdc.noaa.gov/stp/satellite/goes/dataaccess.html)**. We would like to acknowledge high-performance computing support from Cheyenne (doi:10.5065/D6RX99HX) provided by NCAR's Computational and Information Systems Laboratory. This material is based upon work supported by the National Center for Atmospheric Research, which is a major facility sponsored by the National Science Foundation under Cooperative Agreement No. 1852977. We thank the International Space Science Institute for facilitating discussions related to this paper as part of the International Team "An Exploration of the Valley Region in the Low Latitude Ionosphere: Response to Forcing from Below and Above and Relevance to Space Weather". The participation of J. L. C. in this work is part of the project supported by the Deutsche Forschungsgemeinschaft (DFG, German Research Foundation) under SPP 1788 (DynamicEarth)-CH 1482/1-2 (DYNAMITE2).

References

Annadurai, N. M. N., Hamid, N. S. A., Yamazaki, Y., & Yoshikawa, A. (2018). Investigation of Unusual Solar Flare Effect on the Global Ionospheric Current System. *J. Geophys. Res. Sp. Phys.*, *123*(10), 8599–8609. doi: 10.1029/2018JA025601

Balsley, B. B. (1964). Evidence of a stratified echoing region at 150 kilometers in the vicinity of the magnetic equator during daylight hours. *J. Geophys. Res.*, *69*(9), 1925–1930. doi: 10.1029/JZ069i009p01925

Chamberlin, P. C., Woods, T. N., & Eparvier, F. G. (2008). Flare Irradiance Spectral Model (FISM): Flare component algorithms and results. *Sp. Weather*, *6*(5). doi: 10.1029/2007SW000372

Chau, J., Woodman, R., Milla, M., & Kudeki, E. (2009). Naturally enhanced ion-line spectra around the equatorial 150-km region. *Ann. Geophys*, *27*, 933–942.

Chau, J. L. (2004). Unexpected spectral characteristics of VHF radar signals from 150-km region over Jicamarca. , *31*, L23803, doi:10.1029/2004GL021620.

Chau, J. L., & Kudeki, E. (2006). Statistics of 150-km echoes over Jicamarca based on low-power VHF observations. *Ann. Geophys.*, *24*(5), 1305–1310. doi: 10.5194/angeo-24-1305-2006

Chau, J. L., & Kudeki, E. (2013). Discovery of two distinct types of equatorial 150 km radar echoes. *Geophysical Research Letters*, *40*(17), 4509-4514. Retrieved from `https://agupubs.onlinelibrary.wiley.com/doi/abs/`

10.1002/grl.50893 doi: 10.1002/grl.50893

Chau, J. L., Kudeki, E., & Milla, M. (2009). Multi-frequency radar studies of the equatorial 150-km region. In N. Swarnalingam & W. K. Hocking (Eds.), *Proceedings of the 12th international symposium on equatorial aeronomy* (p. 165-168). London, Ontario, Canada.

Choudhary, R. K., St.-Maurice, J.-P., & Mahajan, K. K. (2004). Observation of coherent echoes with narrow spectra near 150 km altitude during daytime away from the dip equator. *Geophys. Res. Lett.*, *31*(19). doi: 10.1029/2004GL020299

de Paula, E. R., & Hysell, D. L. (2004). The São Luís 30 MHz coherent scatter ionospheric radar: System description and initial results. *Radio Sci.*, *39*(1). Retrieved from https://agupubs.onlinelibrary.wiley.com/doi/abs/10.1029/2003RS002914 doi: 10.1029/2003RS002914

Gelaro, R., McCarty, W., Suárez, M. J., Todling, R., Molod, A., Takacs, L., ... Zhao, B. (2017). The Modern-Era Retrospective Analysis for Research and Applications, Version 2 (MERRA-2). *J. Clim.*, *30*(14), 5419–5454. doi: 10.1175/JCLI-D-16-0758.1

Heelis, R. A., Lowell, J. K., & Spiro, R. W. (1982). A model of the high-latitude ionospheric convection pattern. *J. Geophys. Res. Sp. Phys.*, *87*(A8), 6339–6345. doi: 10.1029/JA087iA08p06339

Kudeki, E., & Fawcett, C. D. (1993). High resolution observations of 150 km echoes at Jicamarca. *Geophys. Res. Lett.*, *20*(18), 1987–1990. doi: 10.1029/93GL01256

Kudeki, E., Fawcett, C. D., Ecklund, W. L., Johnston, P. E., & Franke, S. J. (1998). Equatorial 150-km irregularities observed at Pohnpei. *Geophys. Res. Lett.*, *25*(21), 4079–4082. doi: 10.1029/1998GL900069

Lehmacher, G., Lu, X., Kudeki, E., Reyes, P. M., & Milla, M. (2018, May). Simultaneous observations of 150-km echoes and ionosonde virtual heights at jicamarca. In *Proceedings of the 12th international workshop on technical and scientific aspects of mst radar.* Ahmedabad, India.

Lehmacher, G. A., Kudeki, E., Akgiray, A., Guo, L., Reyes, P., & Chau, J. (2009). Radar cross sections for mesospheric echoes at jicamarca. *Annales Geophysicae*, *27*(7), 2675–2684. Retrieved from https://www.ann-geophys.net/27/2675/2009/ doi: 10.5194/angeo-27-2675-2009

Lehmacher, G. A., Kudeki, E., Reyes, P. M., Lee, K., Heale, C. J., & Snively, J. B. (2019). Gravity wave ducting observed in the mesosphere over jicamarca, peru. *Journal of Geophysical Research: Atmospheres*, *124*(10), 5166-5177. Retrieved from https://agupubs.onlinelibrary.wiley.com/doi/abs/10.1029/2019JD030264 doi: 10.1029/2019JD030264

Liu, H.-L., Bardeen, C. G., Foster, B. T., Lauritzen, P., Liu, J., Lu, G., ... Wang, W. (2018). Development and Validation of the Whole Atmosphere Community Climate Model With Thermosphere and Ionosphere Extension (WACCM-X 2.0). *J. Adv. Model. Earth Syst.*, *10*(2), 381–402. doi: 10.1002/2017MS001232

Liu, J., Liu, H., Wang, W., Burns, A. G., Wu, Q., Gan, Q., ... Schreiner, W. S. (2018). First Results From the Ionospheric Extension of WACCM-X During the Deep Solar Minimum Year of 2008. *J. Geophys. Res. Sp. Phys.*, *123*(2), 1534–1553. doi: 10.1002/2017JA025010

Marsh, D. R., Mills, M. J., Kinnison, D. E., Lamarque, J. F., Calvo, N., & Polvani, L. M. (2013). Climate change from 1850 to 2005 simulated in CESM1(WACCM). *J. Clim.*. doi: 10.1175/JCLI-D-12-00558.1

Neale, R. B., Richter, J., Park, S., Lauritzen, P. H., Vavrus, S. J., Rasch, P. J., & Zhang, M. (2013). The Mean Climate of the Community Atmosphere Model (CAM4) in Forced SST and Fully Coupled Experiments. *J. Clim.*. doi: 10.1175/JCLI-D-12-00236.1

Oppenheim, M. M., & Dimant, Y. S. (2016). Photoelectron-induced waves: A likely

source of 150 km radar echoes and enhanced electron modes. *Geophys. Res. Lett.*, *43*(8), 3637–3644. doi: 10.1002/2016GL068179

Patra, A., Pavan Chaitanya, P., St-Maurice, J.-P., Otsuka, Y., Yokoyama, T., & Yamamoto, M. (2017). The solar flux dependence of ionospheric 150 km radar echoes and implications. *Geophysical Research Letters*, *44*(22).

Patra, A. K., Pavan Chaitanya, P., & Tiwari, D. (2011). Characteristics of 150 km echoes linked with solar eclipse and their implications to the echoing phenomenon. *J. Geophys. Res. Sp. Phys.*, *116*(A5). doi: 10.1029/2010JA016258

Patra, A. K., Yokoyama, T., Otsuka, Y., & Yamamoto, M. (2008). Daytime 150-km echoes observed with the Equatorial Atmosphere Radar in Indonesia: First results. *Geophys. Res. Lett.*, *35*(6). doi: 10.1029/2007GL033130

Perkins, F., Salpeter, E., & Yngvesson, K. (1965). Incoherent scatter from plasma oscillations in the ionosphere. *Physical Review Letters*, *14*(15), 579.

Pettit, J., Randall, C. E., Marsh, D. R., Bardeen, C. G., Qian, L., Jackman, C. H., ... Harvey, V. L. (2018). Effects of the September 2005 Solar Flares and Solar Proton Events on the Middle Atmosphere in WACCM. *J. Geophys. Res. Sp. Phys.*. doi: 10.1029/2018JA025294

Qian, L., Burns, A. G., Chamberlin, P. C., & Solomon, S. C. (2011). Variability of thermosphere and ionosphere responses to solar flares. *J. Geophys. Res. Sp. Phys.*, *116*(A10). doi: 10.1029/2011JA016777

Qian, L., Burns, A. G., Solomon, S. C., & Chamberlin, P. C. (2012). Solar flare impacts on ionospheric electrodyamics. *Geophys. Res. Lett.*, *39*(6). doi: 10.1029/2012GL051102

Reyes, P. (2012). *Solar Flare Effects Observed Over Jicamarca During MST-ISR Experiments* (Master of Science, University of Illinios at Urbana-Champaign). Retrieved from `http://hdl.handle.net/2142/31196`

Reyes, P. (2017). *Study of Waves Observed in the Equatorial Ionospheric Valley Region using Jicamarca ISR and VIPIR Ionosonde* (Doctor of Philosophy, University of Illinois at Urbana-Champaign). Retrieved from `http://hdl.handle.net/2142/98349`

Richmond, A. D., Ridley, E. C., & Roble, R. G. (1992). A thermosphere/ionosphere general circulation model with coupled electrodynamics. *Geophys. Res. Lett.*, *19*(6), 601–604. doi: 10.1029/92GL00401

Roble, R. G., Ridley, E. C., Richmond, A. D., & Dickinson, R. E. (1988). A coupled thermosphere/ionosphere general circulation model. *Geophys. Res. Lett.*, *15*(12), 1325–1328. doi: 10.1029/GL015i012p01325

Smith, A. K., Pedatella, N. M., Marsh, D. R., & Matsuo, T. (2017). On the Dynamical Control of the Mesosphere–Lower Thermosphere by the Lower and Middle Atmosphere. *J. Atmos. Sci.*, *74*(3), 933–947. doi: 10.1175/JAS-D-16-0226.1

Tsunoda, R. T., & Ecklund, W. L. (2008). On the sheet-like nature of 150 km (F1) radar echoes. *Geophys. Res. Lett.*, *35*(5). doi: 10.1029/2007GL032152

Zhang, R., Liu, L., Le, H., & Chen, Y. (2017). Equatorial ionospheric electrodynamics during solar flares. *Geophys. Res. Lett.*, *44*(10), 4558–4565. doi: 10.1002/2017GL073238